Supporting Information

A Vinylene-Linked Covalent Organic Framework with Optimized Functional Sites for Efficient C_2H_2/C_2H_4 Separation

Shujie Qiao, Xiuyue He, Kaifeng Liao, Mingshuan Yang, Jun Wang, and Zhiyong Guo*

College of Materials Science and Engineering, Fuzhou University, Fuzhou, Fujian Province 350108, China

Content

1. Materials

Acetone, methanol, tetrahydrofuran, N, N'-dimethylformamide (DMF) and hexane etc. were purchased from Sinopharm National Medicine Corporation. $NiCl_2 \cdot 6H_2O$, Zn powder, triphenylphosphine (PPh_3), 1,4-diformylbenzene, 4,6-dimethyl-2-chloropyrimidine, 4-chloro-2,6-dimethylpyridine and benzoic anhydride were obtained from Adamas-Beta. NMR solvents: chloroform-d was purchased from Adamas-Beta. All chemicals were used without further purification.

2. General Methods

2.1 Analytical techniques

Fourier Transform Infrared (FT-IR) spectroscopies were collected on a Nicolet iS50 Spectrometer with ATR module. ^{13}C Cross Polarization/Magic Angle Spinning Nuclear Magnetic Resonance (CP/MAS NMR) spectra of FZU-98 were recorded on Bruker Advance III 500 nuclear magnetic resonance spectrometer (11.7 T, 500MHz). ^{1}H Nuclear Magnetic Resonance spectra were recorded on AVANCE NEO 600 nuclear magnetic resonance spectrometer (17.1 T, 600 MHz) or AVANCE III/ WB-400 nuclear magnetic resonance spectrometer (9.4 T, 400 MHz). High-Resolution Transmission Electron Microscopy (HR-TEM) images of FZU-98 were gotten in A JEM-2100Plus (LaB6 filament) operated at 200 kV. Thermogravimetric Analyses (TGA) were carried out on NETZSCH STA449-F5 by heating samples from 35 ^{o}C to 800 ^{o}C under nitrogen atmosphere with a heating rate of 10 ^{o}C/min and a gas flow rate of 10 mL/min. Powder X-Ray Diffraction (PXRD) data were obtained on a Rigaku Miniflex 600 diffractometer using Cu Kα radiation (λ = 0.15406 nm). Nitrogen adsorption-desorption analysis and C_2H_2、C_2H_4 sorption measurements were carried out using a Micromeritics 2020 Plus. Before C_2H_2 and C_2H_4 adsorption measurements, all samples were degassed on an outgasser station for 12 h at 120 °C. Structural modeling of FZU-98 was generated using the Accelrys Materials Studio software package. The lattice model was geometry optimized using the Forcite module. Pawley refinement was applied to define the lattice parameters, and relative total energy (RTE) was calculated from COMPASS II Forcite module of Materials Studio 8.0.

2.2 Breakthrough experiments

The breakthrough separation experiments were conducted in a home-built breakthrough apparatus under ambient conditions (298 K, 1 atm) using a gas mixture

of C_2H_2/C_2H_4 (1/99, v/v). In a typical breakthrough experiment test, 0.188 g activated samples FZU-98 were packed into a stainless-steel column (4 mm inner diameter, 100 mm length) and purged with He flow (10 mL/min) at 120 ℃ for 24 h. During tests, the gas mixture of C_2H_2/C_2H_4 was stabilized at 2 mL/min by a mass flow controller at room temperature. Outlet gas from the column was monitored using gas chromatography (GC-9860-5CNJ) continuously. To evaluate the reusability of the adsorbent, the adsorbent was regenerated in-situ by heating for 5 hours with He flow (10 mL/min) at 100 ℃ to finish 3 cycles.

The dynamic uptake of each component was estimated by integrating the corresponding breakthrough curve according to the following equation:

$$q_i = \frac{Fy_i p}{mRT}\int_0^{t_s}\left(1 - \frac{C_i}{C_{i,0}}\right)dt$$

where q_i is the dynamic uptake of component i, F is the total volumetric flow rate, y_i is the inlet molar fraction of component i, p is the pressure, m is the mass of adsorbent, R is the gas constant, T is the temperature, and $C_i/C_{i,0}$ is the normalized outlet concentration of component i. The dynamic selectivity was estimated from the ratio of the resulting dynamic uptakes normalized by the feed composition.

2.3 Isosteric Heats of Adsorption (Q_{st})

To extract the coverage-dependent isosteric heat of adsorption, the adsorption data were modeled with a virial-type expression composed of parameters a_i and b_i that are independent of temperature:

$$lnP = lnN + \frac{1}{T}\sum_{i=0}^{m} a_i N^i + \sum_{i=0}^{m} b_i N^i$$

where *P* is pressure, *N* is the amount adsorbed (or uptake), *T* is temperature and m and n determine the number of terms required to adequately describe the isotherm.

$$Q_{st} = -R\sum_{i=0}^{m} a_i N^i$$

where R is the universal gas constant, the coverage dependencies of Q_{st} values were calculated from fitting the adsorption data (under the pressure range from 0-1 bar) at different temperatures for FZU-98 and COF-DFB.

2.4 Fitting of experimental data on pure component isotherms

The single-component adsorption isotherms for C_2H_2 and C_2H_4 of FZU-98 and COF-DFB were calculated by fitting the adsorption isotherms at 298 K for the respective adsorbates to the Dual-Site Langmuir-Freundlich (DSLF) equation.
The DSLF equation was given by:

$$q = q_1 \frac{b_1 p^{1/n_1}}{1 + b_1 p^{1/n_1}} + q_2 \frac{b_2 p^{1/n_2}}{1 + b_2 p^{1/n_2}}$$

where p is the bulk gas pressure at equilibrium with the adsorbed phase (kPa), q is the adsorbed amount per mass of adsorbent (mmol g^{-1}), q_1 and q_2, b_1 and b_2 are the saturation capacities (mmol g^{-1}) and affinity coefficients (kPa^{-1}) of sites 1 and 2, respectively. n_1 and n_2 are the deviations from an ideal homogeneous surface.

2.5 IAST selectivity calculation

IAST calculations of mixture adsorption were carried out to compare the C_2H_2/C_2H_4 separation performance of FZU-98 and COF-DFB. For the separation of a binary mixture of components A and B, the adsorption selectivity is defined by

$$S_{abs} = \frac{q_A / q_B}{y_A / y_B}$$

2.6 Binding mechanisms calculation

Density functional theory (DFT) calculations were conducted to illustrate the binding mechanisms between C_2 hydrocarbons and COFs. The binding structure of gas molecule (C_2H_2 or C_2H_4) and the repetitive units (COF-DFB or FZU-98) were constructed and optimized for binding energy (BE) calculation with the B3LYP/6-31G(d, p) method. BE between COF structure and gas molecule was defined as BE (ΔE) = $E_{COF + gas\ molecule}$ - E_{COF} − $E_{gas\ molecule}$. The negative value of BE demonstrates that gas adsorption process is an exothermic adsorption and its absolute value is positively correlated with the adsorption strength between framework and gas.

3. Syntheses

3.1 Synthesis of 4,4',6,6'-tetramethyl-2,2'-bipyrimidine (TMBM).

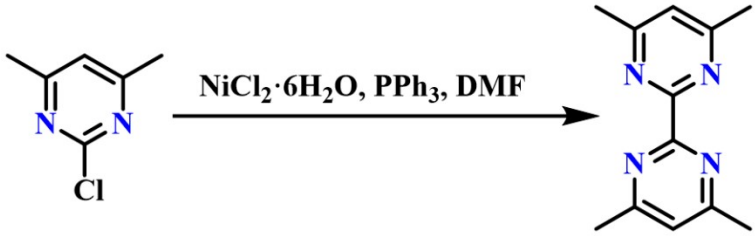

Under N_2 atmosphere, A mixture of $NiCl_2 \cdot 6H_2O$ (8.33 g, 35.1 mmol), PPh_3 (36.81 g, 140 mmol) and DMF solution (160 mL) was added into a 500 mL round-bottled flask and degassed by two freeze pump-thaw cycles. Zinc powder (3.20 g, 49.1 mmol) was added and then repeat one additional freeze-pump-thaw cycle. Then, the suspension was stirred for one hour at room temperature. Subsequently, 4,6-dimethyl-2-chloropyrimidine (5.00 g, 35.1 mmol) dissolved in dry DMF (30 mL) was added to the suspension and then refluxed at 70 °C for 24 hours. After cooling to room temperature, ammonia (4M, 640 mL) was poured into the mixture. After stirring for 30 minutes at ambient temperature, the precipitate was filtered off and the filtrate solution was extracted with CH_2Cl_2. When the extraction (CH_2Cl_2) was dried over $MgSO_4$ and evaporated, the residue was further purified by column chromatograph (CH_2Cl_2: MeOH = 24:1, detection: UV) to yield a yellow solid (2.26 g, 60%). ^1H NMR (400 MHz, $CDCl_3$) δ = 7.15 (s, 2 H), 2.66 (s, 12 H) ppm.

3.2 Synthesis of 2,2',6,6'-tetramethyl-4,4'-bipyridine (TMBP).

2,2',6,6'-tetramethyl-4,4'-bipyridine was prepared according to the reported literature[1].

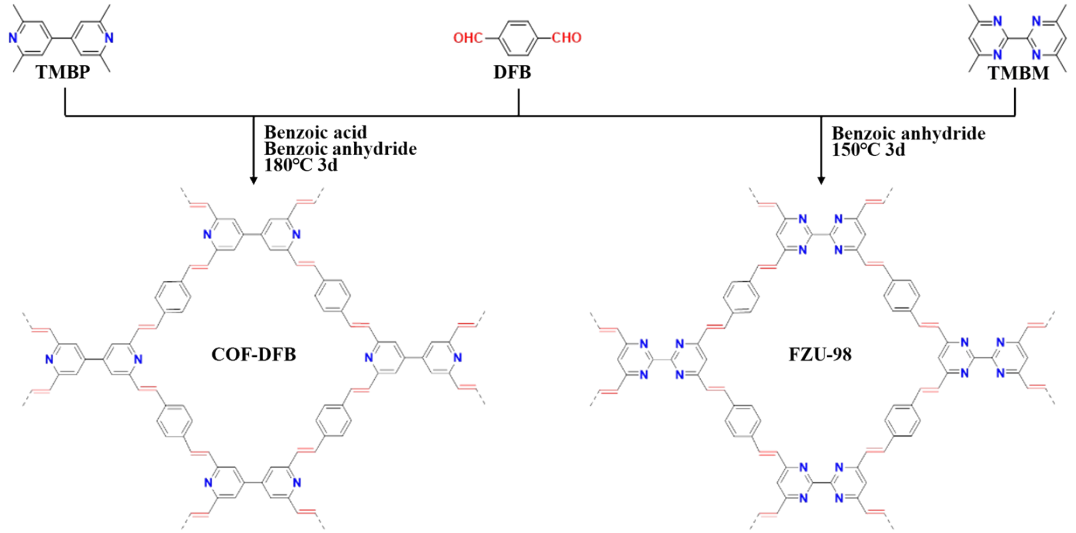

3.3 Synthesis of FZU-98

A 5 mL Pyrex tube was charged with 4,4',6,6'-tetramethyl-2,2'-bipyrimidine (42.8

mg, 0.2 mmol), 1,4-diformylbenzene (53.7 mg, 0.4 mmol) and benzoic anhydride (90.5 mg, 0.4 mmol). After frozen at 77 K and degassed through three freeze-pump-thaw cycles, the tube was sealed under vacuum. Then the mixture was heated at 150 ℃ for 3 days. After cooling to room temperature, the resulting precipitate was collected by filtration and then washed with acetone, tetrahydrofuran and methanol. The product was obtained as red powder in 87% yield after Soxhlet extraction with acetone/methanol (v/v = 1/1) for 36 h and then drying at 60℃ for 12 hours under vacuum.

3.4 Synthesis of COF-DFB

COF-DFB was prepared according to the reported literature[1].

4. Proposed Mechanism for Aldol Condensation of Methylpyrimidine and Benzaldehyde.

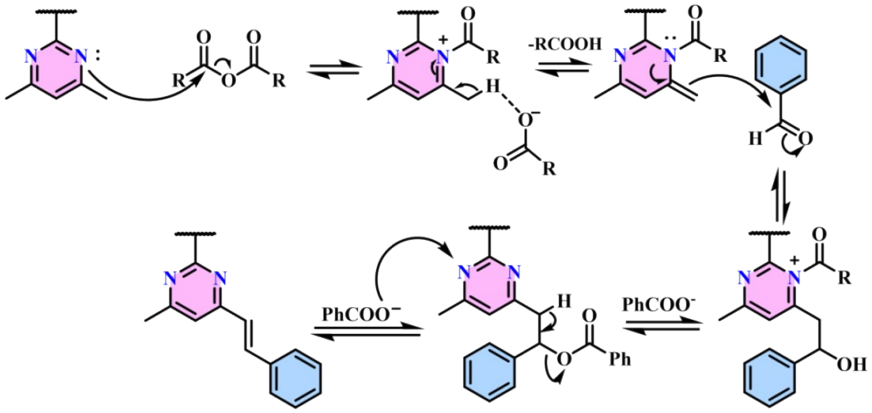

The reasonable mechanism can be proposed as follows (Scheme 2)[1, 3]: First, the nucleophilic substitution reaction between pyrimidine nitrogen and benzoic anhydride could form benzoyl pyrimidine salt, increasing the C-H activity on the pyrimidylmethyl. Subsequently, the activated H atoms of pyrimidylmethyl will further react with benzoate ions to yield enamine intermediate, which will further undergo nucleophilic attack on benzaldehyde to form an enamine molecule containing C-C single bonds and hydroxyl groups. Owing to the cross-reaction among molecule, the hydroxide groups can convert into benzoate, which is a good leaving functional group. Finally, the benzoate ion, as a base, will combine with the protons on the methyl groups via elimination of benzoic acid, which will eventually form carbon-carbon double bonds.

Characterizations

Supplementary Fig.s and Tables

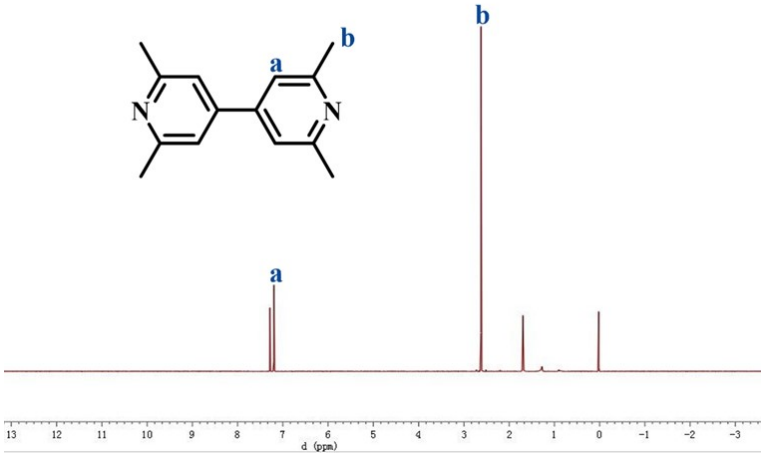

Fig. S1: ^{1}H NMR spectrum of 2,2',6,6'-tetramethyl-4,4'-bipyridine recorded in $CDCl_3$.

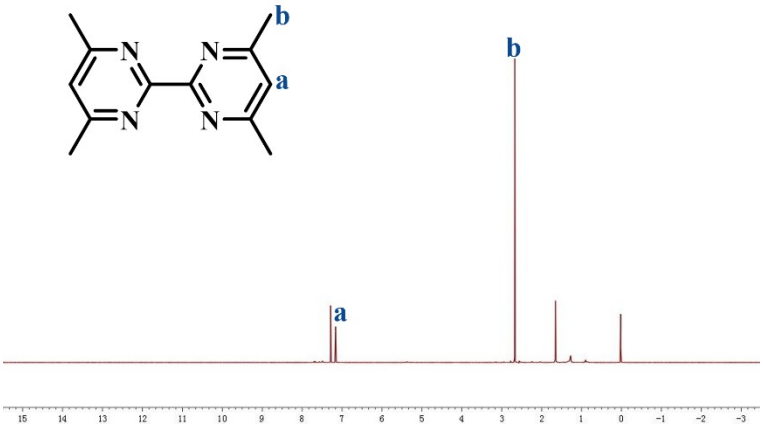

Fig. S2: ^{1}H NMR spectrum of 4,4',6,6'-tetramethyl-2,2'-bipyrimidine recorded in $CDCl_3$.

Table S1: Optimized synthetic conditions for FZU-9

Entry	Catalyst	Solvents	Temperature (°C)	Time (days)	Crystallinity
1	1M/5M NaOH	aliquat 336	180	3	No
2	4M NaOH	MeOH/mesitylene (1:3)	160	3	No
3	4M NaOH	mesitylene/dioxane (4.9:1)	90	3	No
4	Pyridine	DMF/o-DCB (10:1)	180	3	No
5	Pyridine	DMF	150	3	No
6	Pyridine	DMAC/o-DCB (1:1)	180	5	No
7	Cs_2CO_3	o-DCB	150	3	No
8	Cs_2CO_3	o-DCB/n-BuOH (7:3) / (1:1)	120	3	No
9	Ac_2O	No	180/200	3	No
10	benzoic anhydride	No	150	3	Moderate
11	benzoic anhydride	No	180	3	Low
12	benzoic anhydride	No	200	3	Low
13	benzoic anhydride	No	220/240	3	No
14	benzoic anhydride benzoic acid	No	180/200	3	Low
15	trifluoroacetic acid	CH_3CN/mesitylene/ dioxane (1:18:18)	150	3	Low
16	trifluoroacetic acid	CH_3CN/mesitylene/ dioxane (1:18:18)	120	7	No
17	HAc	mesitylene	180	5	No
18	HAc	o-DCB/n-BuOH (1:1)	120	3	No
19	HAc	DMAC/o-DCB (1:1)	180	5	No
20	$ZnCl_2$	No	220	3	No
21	$ZnCl_2$	ethanol/dioxane (2:3)	100	3	No

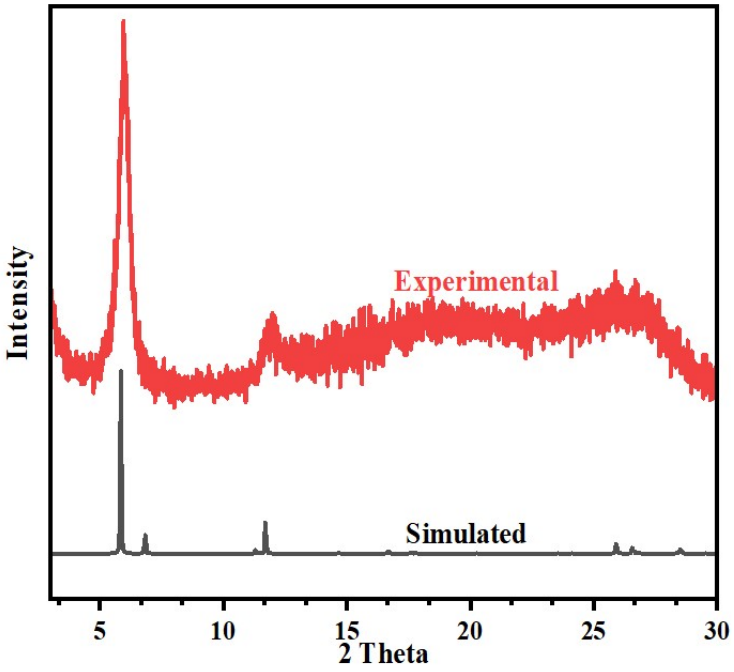

Fig. S3: Experimental and simulated PXRD patterns for COF-DFB.

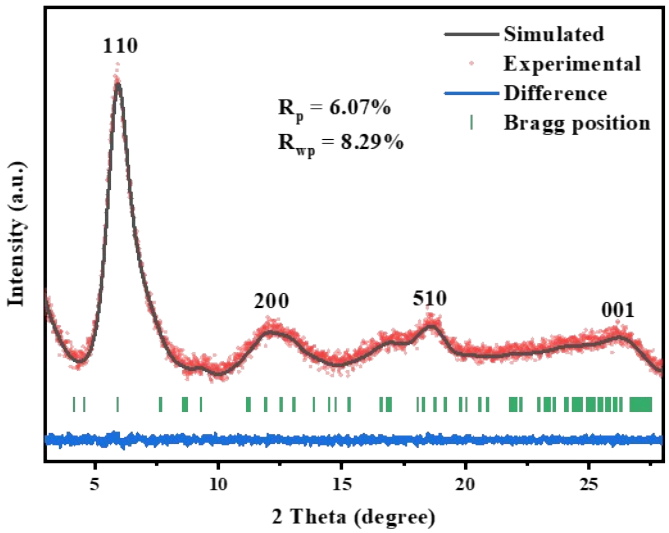

Fig. S4: PXRD patterns and Pawley refinement of FZU-98. Experiment data, simulated results of AA-Stacking, difference plot and Bragg position were marked as red, black, blue and green respectively.

As shown in Fig. S4, the experimental PXRD pattern of FZU-98 was reasonably consistent with the calculated results from the AA-stacking mode. Additionally, the profile of the Pawley refinement matched well with the AA-stacking, which can be evident by their negligible deviation with R_{wp} and R_p converged to 8.29% and 6.07%, respectively.

Table S2: The Space Groups, Cell Parameters and RTE[a] the of the two possible structures of FZU-98

Structure	Crystal system	Space Group	Cell Parameters	RTE (Kcal/J)
AA-stacking	Orthorhombic	*Cmmm*	a = 23.97 Å, b = 21.21 Å, c = 3.44 Å, α = β = γ =90°	632.47
AB-stacking	Orthorhombic	*Cmcm*	a = 23.97 Å, b = 21.21 Å, c = 6.88 Å, α = β = γ =90°	1288.92

[a]RTE: relative total energy. Calculated by COMPASS II in the Forcite module of Materials Studio 8.0.

Among diverse stacking modes, the total energy of the AA-stacking was the lowest, suggesting that AA-stacking model is energetically favorable.

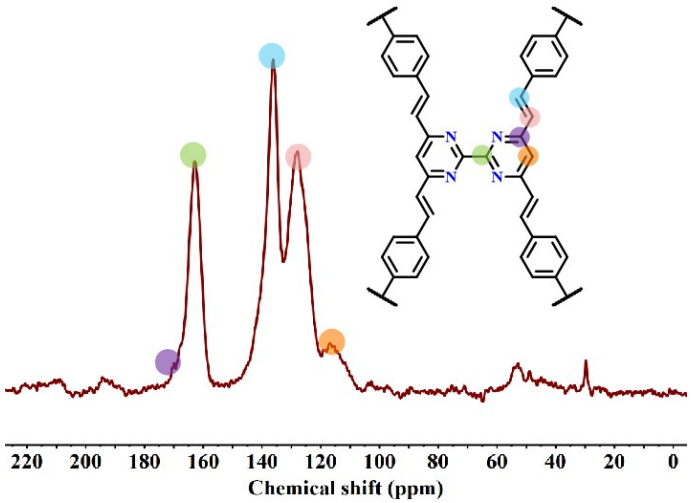

Fig. S5: ^{13}C CP/MAS solid-state NMR spectra (full spectra) of FZU-98.

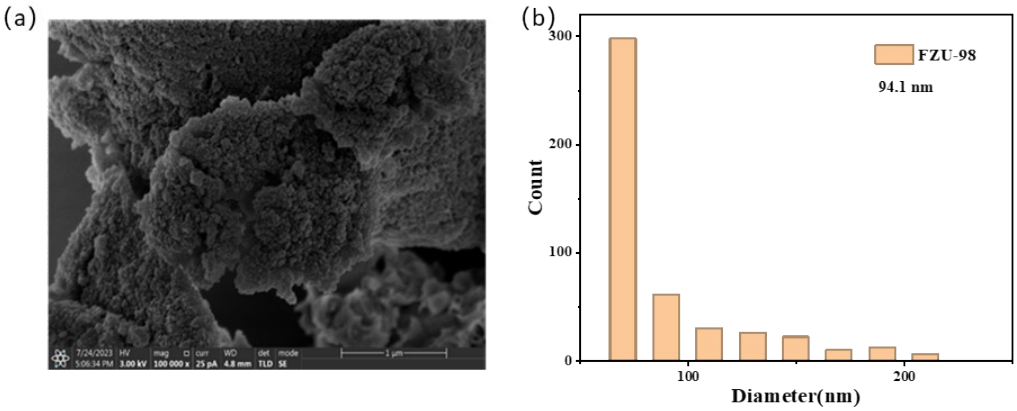

Fig. S6: (a) SEM image of FZU-98. (b) Particle-size distribution histogram of FZU-98 estimated from the SEM image.

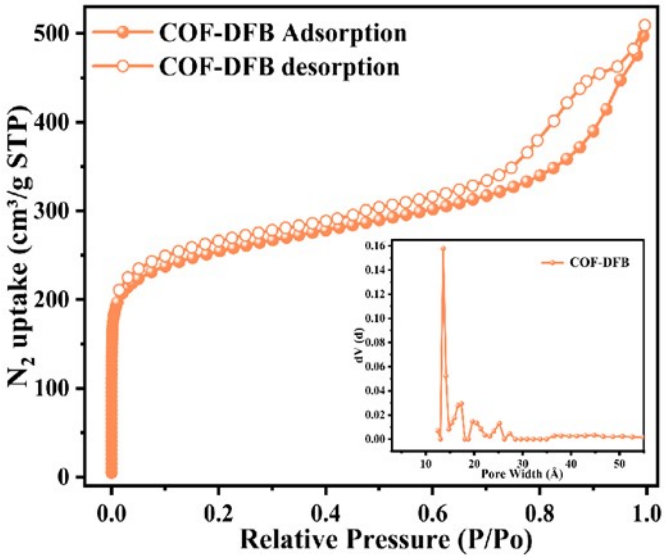

Fig. S7: Nitrogen sorption isotherms of COF-DFB. Inset: pore size distribution calculated from nonlocal density functional theory.

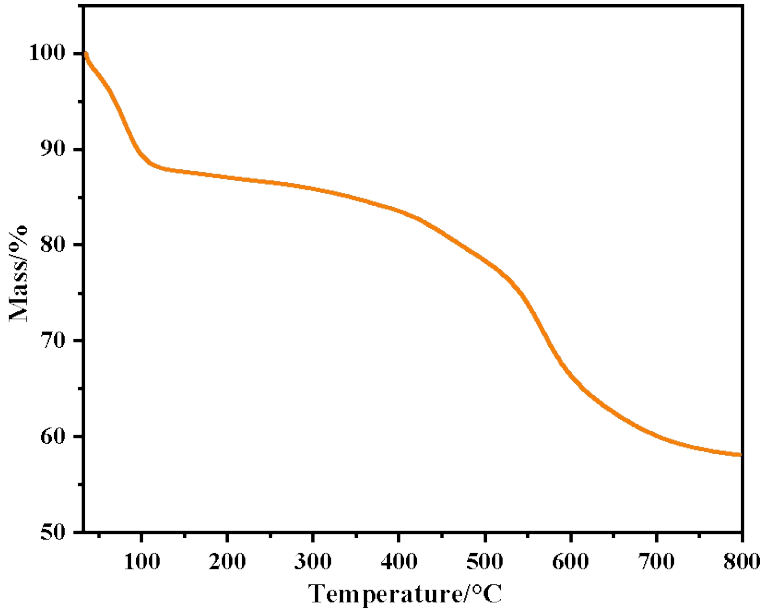

Fig. S8: TGA curve of FZU-98.

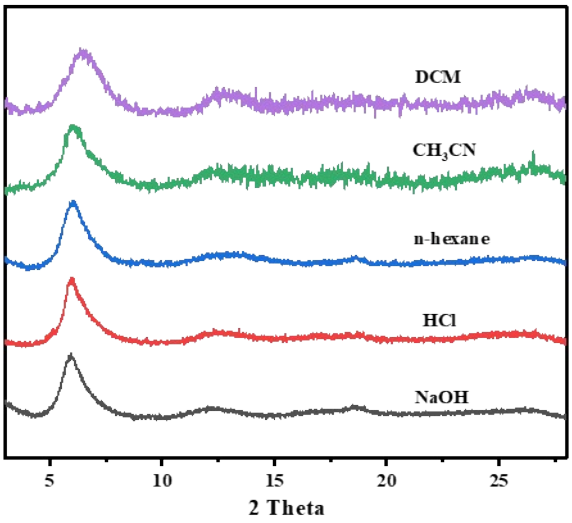

Fig. S9: PXRD patterns of FZU-98 after chemical stability tests in different solvents.

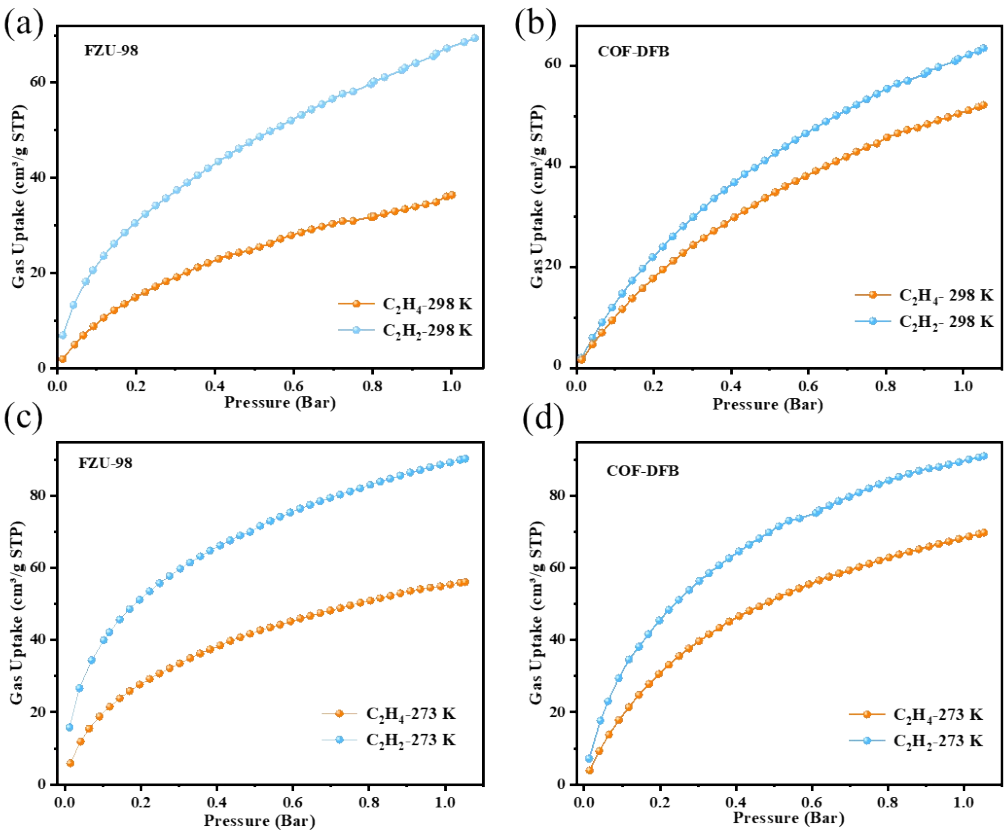

Fig. S10: Gas adsorption isotherms of FZU-98 and COF-DFB for C_2H_2 and C_2H_4 at 298 K (a, b) and 273 K (c, d).

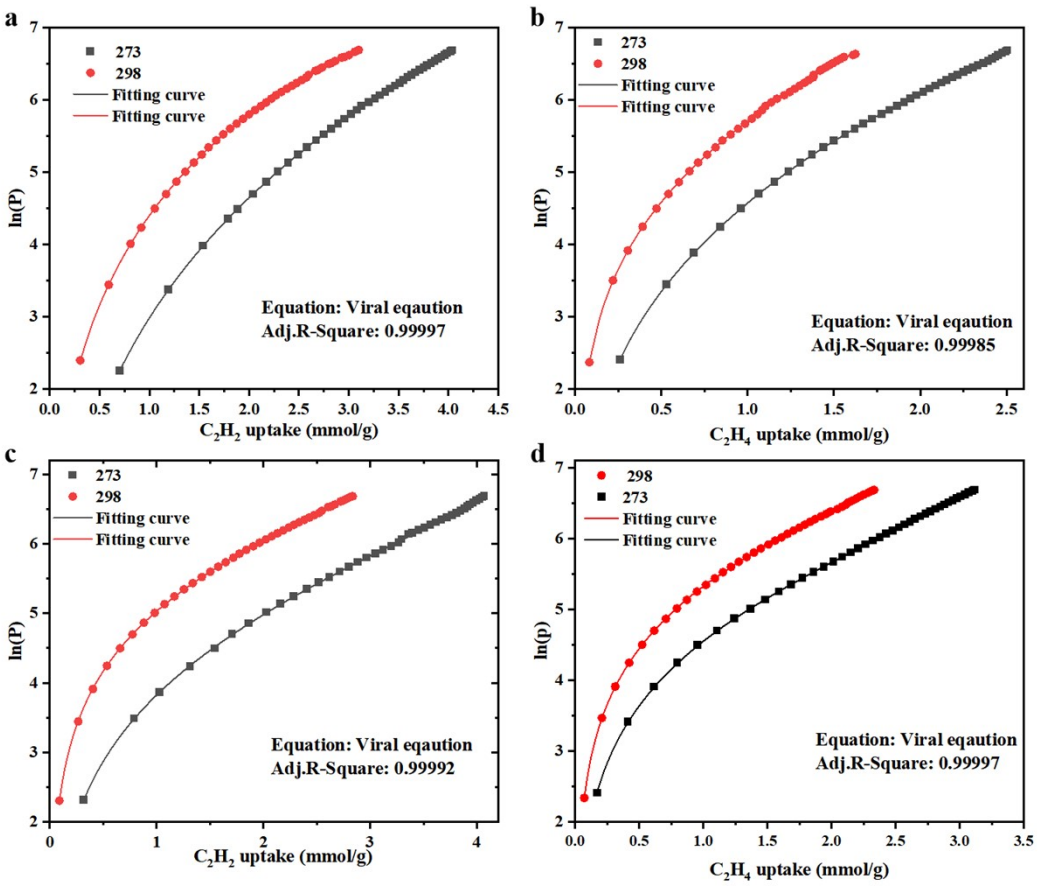

Fig. S11: Virial equation fitting of C_2H_2 (a, c) and C_2H_4 (b, d) adsorption isotherms of FZU-98 (a,b) and COF-DFB (c, d).

Table S3: The fitted parameters of the Dual-Site Langmuir-Freundlich (DSLF) equation for FZU-98.

Parameter	C_2H_4	C_2H_2
q_1	1.78853	15.38401
b_1	0.02149	0.00943
$1/n_1$	0.78301	0.52793
q_2	1.78853	15.38401
b_2	0.02149	0.00943
$1/n_2$	0.78301	0.52793
R^2	0.99925	0.99972

Table S4: The fitted parameters of the Dual-Site Langmuir-Freundlich (DSLF) equation for COF-DFB.

Parameter	C_2H_4	C_2H_2
q_1	2.43035	2.9771
b_1	0.01182	0.01293
$1/n_1$	0.93311	0.90977
q_2	2.43035	2.9771
b_2	0.01182	0.01293
$1/n_2$	0.93311	0.90977
R^2	0.99993	0.99997

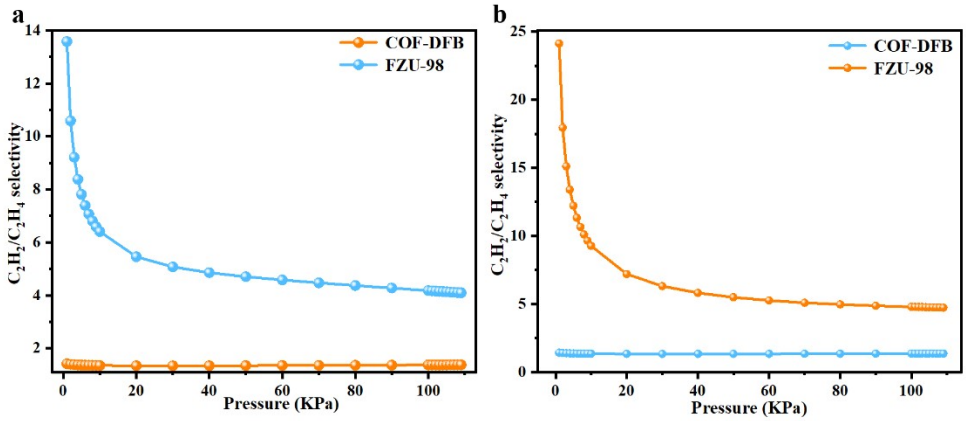

Fig. S12: IAST selectivity of C_2H_2/C_2H_4 (1:1, v/v) and C_2H_2/C_2H_4 (1:99, v/v) mixture for FZU-98 and COF-DFB at 298 K.

Table S5: Comparison of adsorbents in C_2H_2/C_2H_4 separation under ambient conditions.

Porous Materials	Adsorption uptake (cm^3/g, 298 K)		IAST selectivity	Q_{st}		Ref.
	C_2H_2	C_2H_4	C_2H_2/C_2H_4 (1/99)	C_2H_2	C_2H_4	
Tp-ND	53	35	3.1	32.8	27.6	4
TFB-IQD	11	6	3.5	20	14.6	
TP-IQD	46	16	13.8	33.8	21.7	
PAF-110	54.53	1.29	8	38.4	22.6	5
PAF-120	55.50	1.22	4.1	37.5	34.3	6
NKCOF-62	55.80	44.8	1.37	30.5	29.6	2
COF-ECUT-1	55.39	28.63	6.33	7.68	15.9	7
P5-COF	-	-	3.2	-	-	8
NKCOF-11-AA	42.4	28.3	2.5	28.0	27.0	9
NKCOF-11-ABC	68.0	45.7	2.4	30.8	28.1	
CTF-PO71	74	-	2.8	28	22	10
FZU-98	69.5	36.5	4.9	41.7	35.9	**This work**
COF-DFB	63.8	52.2	1.4	30.8	21.5	
UiO-67-$(NH_2)_2$	132.2	96.8	2.1	27.4	24.5	11
$CuTiF_6$-TPPY	88.51	59.17	5.03	36.5	29.6	12
MOF-525	64.55	66.02	1.44(10:90)	15.81	16.74	13
UPC-612	67.4	65.3	1.07	23.94	16.94	

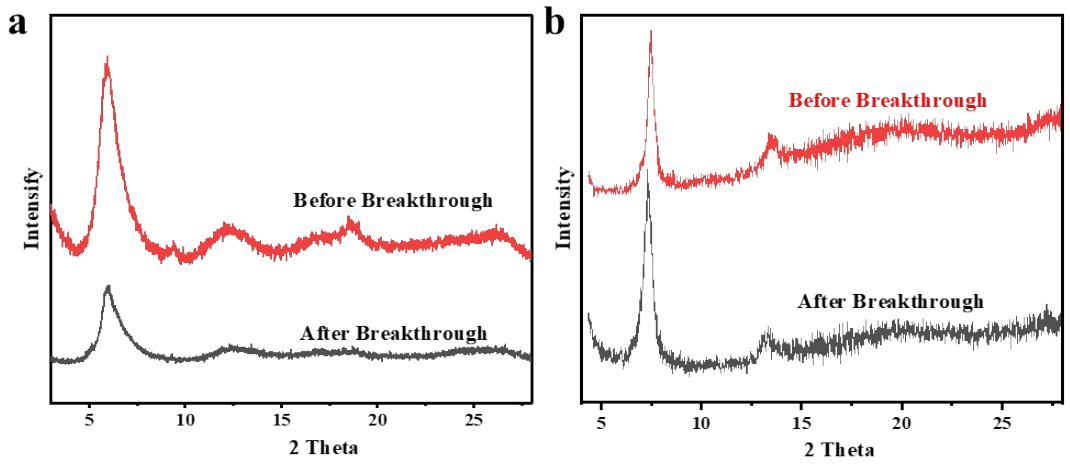

Fig. S13: The PXRD patterns contrast of FZU-98 (a) and COF-DFB (b) before and after breakthrough test.

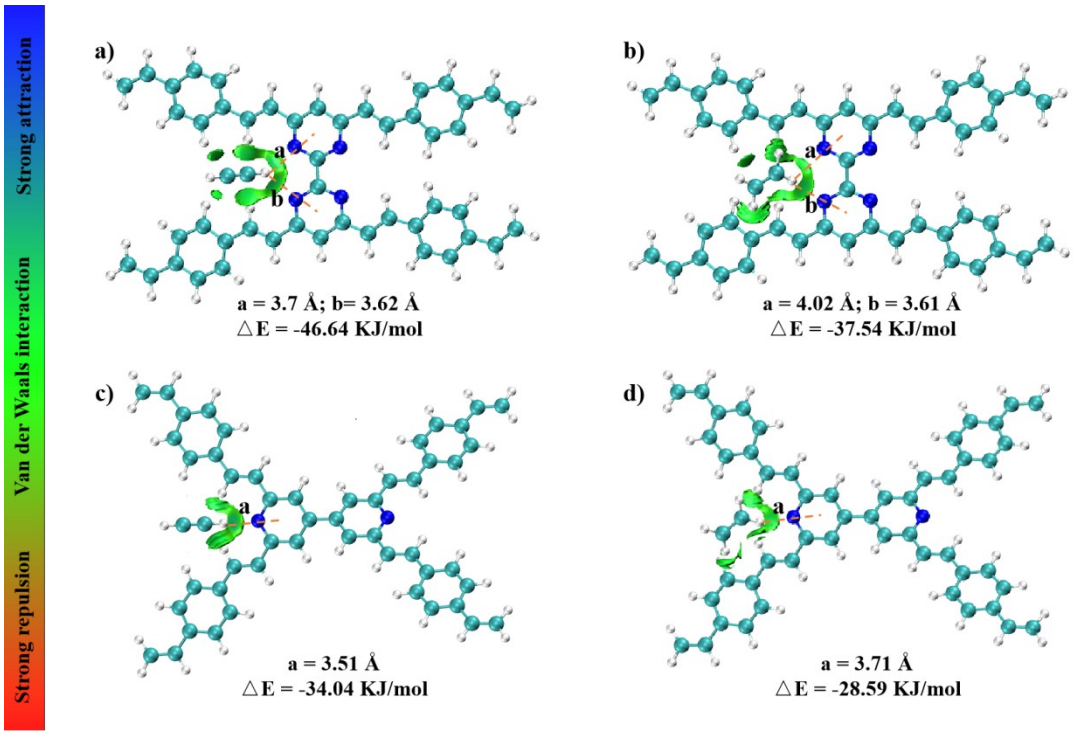

Fig. S14: The C−H…π binding distance and binding energies for C_2H_2 (a, c) and C_2H_4 (b, d) within FZU-98 (a, b) and COF-DFB (c, d), respectively.

References

1. S. Bi, F. Meng, D. Wu and F. Zhang, *J. Am. Chem. Soc.*, 2022, **144**, 3653-3659.

2. Z. Wang, Y. Zhang, E. Lin, S. Geng, M. Wang, J. Liu, Y. Chen, P. Cheng and Z. Zhang, *J. Am. Chem. Soc.*, 2023, **145**, 21483-21490.

3. S. Li, R. Ma, S. Xu, T. Zheng, G. Fu, Y. Wu, Z. Liao, Y. Kuang, Y. Hou, D. Wang, P. S. Petkov, K. Simeonova, X. Feng, L. Z. Wu, X. B. Li and T. Zhang, *J. Am. Chem. Soc.*, 2022, **144**, 13953-13960.

4. J. Li, Z. Cheng, Z. Wang, J. Dong, H. Jiang, W. Wang, X. Zou and G. Zhu, *Angew. Chem. Int. Ed.*, 2023, **62**, e202216675.

5. G. H. V. Bertrand, V. K. Michaelis, T.-C. Ong, R. G. Griffin and M. Dincă, *Proc. Natl. Acad. Sci.*, 2013, **110**, 4923-4928.

6. L. Jiang, P. Wang, M. Li, P. Zhang, J. Li, J. Liu, Y. Ma, H. Ren and G. Zhu, *Chem.*, 2019, **25**, 9045-9051.

7. Y. Tao, R. Krishna, L. X. Yang, Y. L. Fan, L. Wang, Z. Gao, J. B. Xiong, L. J. Sun and F. Luo, *Inorg. Chem. Front.*, 2019, **6**, 2921-2926.

8. L. Liu, Y. Hu, S. Huang, Y. Jin, J. Cui, W. Gong and W. Zhang, *Chem. Sci.*, 2021, **12**, 13316-13320.

9. Z. Wang, Y. Zhang, T. Wang, E. Lin, T. Wang, Y. Chen, P. Cheng and Z. Zhang, *Small*, 2023, **19**, e2303684.

10. Y. Lu, J. He, Y. Chen, H. Wang, Y. Zhao, Y. Han and Y. Ding, *Macromol. Rapid Commun.*, 2018, **39**, 1700468.

11. X.-W. Gu, J.-X. Wang, E. Wu, H. Wu, W. Zhou, G. Qian, B. Chen and B. Li, *J. Am. Chem. Soc.*, 2022, **144**, 2614-2623.

12. P. Zhang, Y. Zhong, Y. Zhang, Z. Zhu, Y. Liu, Y. Su, J. Chen, S. Chen, Z. Zeng, H. Xing, S. Deng and J. Wang, *Sci. Adv.*, 2022, **8**, eabn9231.

13. Y. Wang, C. Hao, W. Fan, M. Fu, X. Wang, Z. Wang, L. Zhu, Y. Li, X. Lu, F. Dai, Z. Kang, R. Wang, W. Guo, S. Hu and D. Sun, *Angew. Chem. Int. Ed.*, 2021, **60**, 11350-11358.